ACS OMEGA

Open Access



http://pubs.acs.org/journal/acsodf

Article

# Electrospun Nanofiber Mats with Embedded Zinc Oxysulfide for Photoreduction of Nitrobenzene to Aniline under Mild Condition

Elvri Melliaty Sitinjak,* Indra Masmur,* Poltak Evencus Hutajulu, New Vita Mey Destty Marbun, and Golfrid Gultom

Cite This: *ACS Omega* 2023, 8, 35328−35335

Read Online

ACCESS | Metrics & More | Article Recommendations

**ABSTRACT:** In this work, electrospun nanofiber embedded with zinc oxysulfide (Zn(O,S)) has been demonstrated as an efficient and robust photocatalyst for hydrogenation of nitrobenzene to aniline under solar light irradiation at mild conditions with methanol as the hole scavenger. The solid solution state of Zn(O,S) in electrospun nanofiber was successfully revealed by high-resolution transmission electron microscopy and X-ray diffraction analyses in which the lattice fringes and diffraction planes located in between those of ZnO and ZnS phases. Moreover, the electrochemical and optical properties of Zn(O,S) embedded in polyethylene oxide (PEO) nanofiber are found to be better than those of ZnO and ZnS indicating more efficient photocatalytic activities as well. The photocatalytic hydrogenation of nitrobenzene to aniline occurred completely within 2 h of the photocatalytic reaction with a reusability of 95% after five consecutive runs. Finally, the mechanism of photocatalytic hydrogenation by Zn(O,S) embedded in the PEO (PZOS) nanofiber involves a total of six electrons ($e^-$) and six protons ($H^+$) to hydrogenate nitrobenzene to nitrosobenzene, phenylhydroxylamine, and aniline.

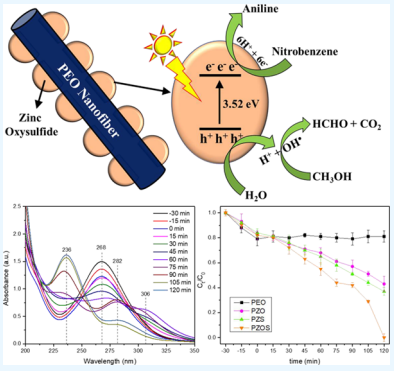


## 1. INTRODUCTION

The chemical contamination in freshwater by organic compounds has been one of the most popular issues. For instance, nitrobenzene has contaminated the environment resulting from practical uses in industries. Nitrobenzene is widely used in industries and is stable due to its aromatic ring. Currently, nitrobenzene can be converted to a more valuable compound, aniline, through a hydrogenation reaction.[1] The hydrogenation reaction of nitrobenzene to aniline was observed in 1854 by a process called Béchamp reduction utilizing iron and hydrochloric acid.[2] As compared to nitrobenzene, aniline possesses relatively low toxicity and is frequently used as a vital precursor in a wide variety of industries (e.g., dyes, consumer goods, pharmaceutical companies, etc.).[3] Generally speaking, contamination by toxic compounds is harmful to our environment and dangerous for human health without proper treatments.

Generally, the hydrogenation reaction from nitrobenzene to aniline is performed at relatively high temperature and high pressure and involves a reducing agent ($NaBH_4$) as reported elsewhere.[4] Some studies also performed the catalytic reduction of nitrobenzene to aniline using platinum group metals (PGMs), which is not economically viable. For instance, Torres et al. (2013) reported the hydrogenation of nitrobenzene using $Au/TiO_2$ and $Au/SiO_2$ catalysts.[5] The work utilized tiny gold particles because Au did not exhibit hydrogen chemisorption capability. Moreover, Moghaddam et al. (2014) synthesized a nano-$Fe_3O_4$@$Al_2O_3$ catalyst on a pressurized flow system at 150 °C and 30 bar back pressure.[6] Moving forward, more sustainable approaches highlighting the principles of mild reaction conditions, green chemistry, and economically friendly methods are urgently required.

Among several methods, catalysis using light illumination as the driving force, so-called photocatalysis has gained researchers' attention owing to its simplicity and unlimited light sources in nature. Even though there are a lot of photocatalysis works have been reported, however, the unsolved challenges still remain. One of the most important factors in the photocatalysis method is the recombination between $e^-$ and hole ($h^+$) as the photocatalysts are irradiated with suitable light sources. This is because the success of reduction or oxidation reactions is highly dependent on these photocarriers.[7] Another factor is the resident time of target compounds occupied at the active surfaces of photocatalysts. In other words, the photocatalysts must exhibit good chemisorption capability. Zinc oxide (ZnO) and zinc sulfide (ZnS) are the most well-known semiconductors due to their

**Received:** July 18, 2023
**Accepted:** August 29, 2023
**Published:** September 15, 2023





https://doi.org/10.1021/acsomega.3c05171
*ACS Omega* 2023, 8, 35328−35335

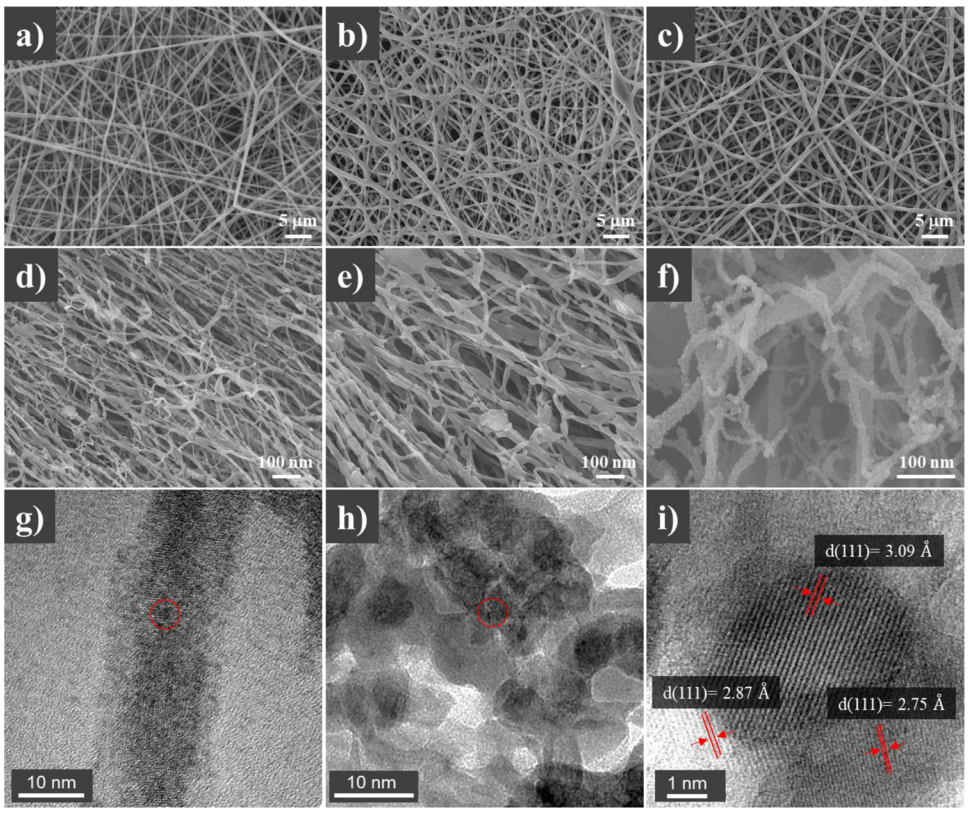


**Figure 1.** SEM images of pristine (a) PZO, (b) PZS, and (c) PZOS nanofibers at low magnification. High-magnification SEM images of (d) PZO annealed at 400 °C, (e) PZS sulfurized at 350 °C, and (f) PZOS partially sulfurized at 350 °C. (g, h) TEM images of PZOS nanofiber at different magnifications with (i) its corresponding high-resolution TEM lattice fringe image.

wide bandgap materials (>3 eV), large exciton binding energy (40−60 meV), and excellent physicochemical properties.[8,9] For optimization purposes, there are several strategies to enhance the photocatalytic activity of catalysts, such as doping processes, solid solution, heterojunction, surface plasmon resonance, etc.[10−13] Solid solution catalysts have been reported to demonstrate excellent catalytic activity as reported elsewhere.[14,15]

With this regard in mind, the authors synthesized and characterized the solid solution of zinc oxysulfide (Zn(O,S)) on a polyethylene oxide (PEO) nanofiber. Herein, the PEO nanofiber was used not only for Zn(O,S) growth substrate to increase the surface-to-volume ratio,[16−19] but also to enhance the chemisorption of nitrobenzene during the photoreaction. The novelty in this study is the fabrication of Zn(O,S) solid solution in the PEO nanofiber for photocatalytic hydrogen evolution reaction (HER) and hydrogenation reaction of azobenzene to aniline under mild conditions which has not been reported previously. The application of Zn(O,S) embedded in the PEO (PZOS) nanofiber was to reduce nitrobenzene to aniline under mild conditions with the assistance of methanol as the hole scavenger.

## 2. MATERIALS AND METHODS

**2.1. Chemicals.** PEO (MW = 200.000), zinc nitrate hexahydrate ($Zn(NO_3)_2{\cdot}6H_2O$, Sigma Aldrich, 98%), and thiourea (Sigma Aldrich, 99%) were used as received without any further purification.

**2.2. Preparation of PZO, PZS, and PZOS Nanofibers.** In a typical experiment, 8 g of PEO was stirred overnight in a solution of 50% ethanol to obtain a viscous solution. A desired amount of $Zn(NO_3)_2$ was added to the viscous solution. Then, the mixture solution was transferred into a syringe tube equipped with a stainless-steel needle (Ø = 0.154 mm), and the electrospinning process was carried out at a constant voltage of 20 kV and a distance of 10 cm between the tip of the needle and drum collector (covered with aluminum foil).[20] The as-electrospun nanofiber was annealed in a muffle furnace at 350 °C for 2 h to obtain a PEO-containing ZnO (PZO) nanofiber. To synthesize ZnS embedded in PEO nanofiber (PZS) and PZOS nanofibers, a desired amount of thiourea was added into the mixture solution prior to the electrospinning process. Subsequently, the as-electrospun nanofibers were annealed under a nitrogen atmosphere at 300 °C to fabricate PZS nanofibers. Meanwhile, for PZOS, the as-electrospun nanofiber was annealed with a controlled gas of oxygen and nitrogen with a 20:80 ratio. The fabricated PZO, PZS, and PZOS nanofibers were carefully stored in an electrical oven at 50 °C for further use.

**2.3. Nanofibers Characterizations.** The morphology of PZO, PZS, and PZOS nanofiber samples was observed using field emission scanning electron microscopy (FESEM, JSM-6500) and field emission gun transmission electron microscopy (FEG-TEM, Tecnai G2 F30). The crystallinity of nanofibers was examined using X-ray diffraction (XRD, D2 phaser) with the $2\theta$ from 15° to 70°. The chemical functionalities of nanofibers was analyzed using Fourier transform infrared (FTIR) analysis; meanwhile, XPS analysis was carried out to determine the chemical states in the composite nanofibers. The optical properties of samples were determined by diffuse reflectance spectroscopy (DRS) and photoluminescence (PL). Further, the electrochemical properties were characterized


https://doi.org/10.1021/acsomega.3c05171
ACS Omega 2023, 8, 35328−35335

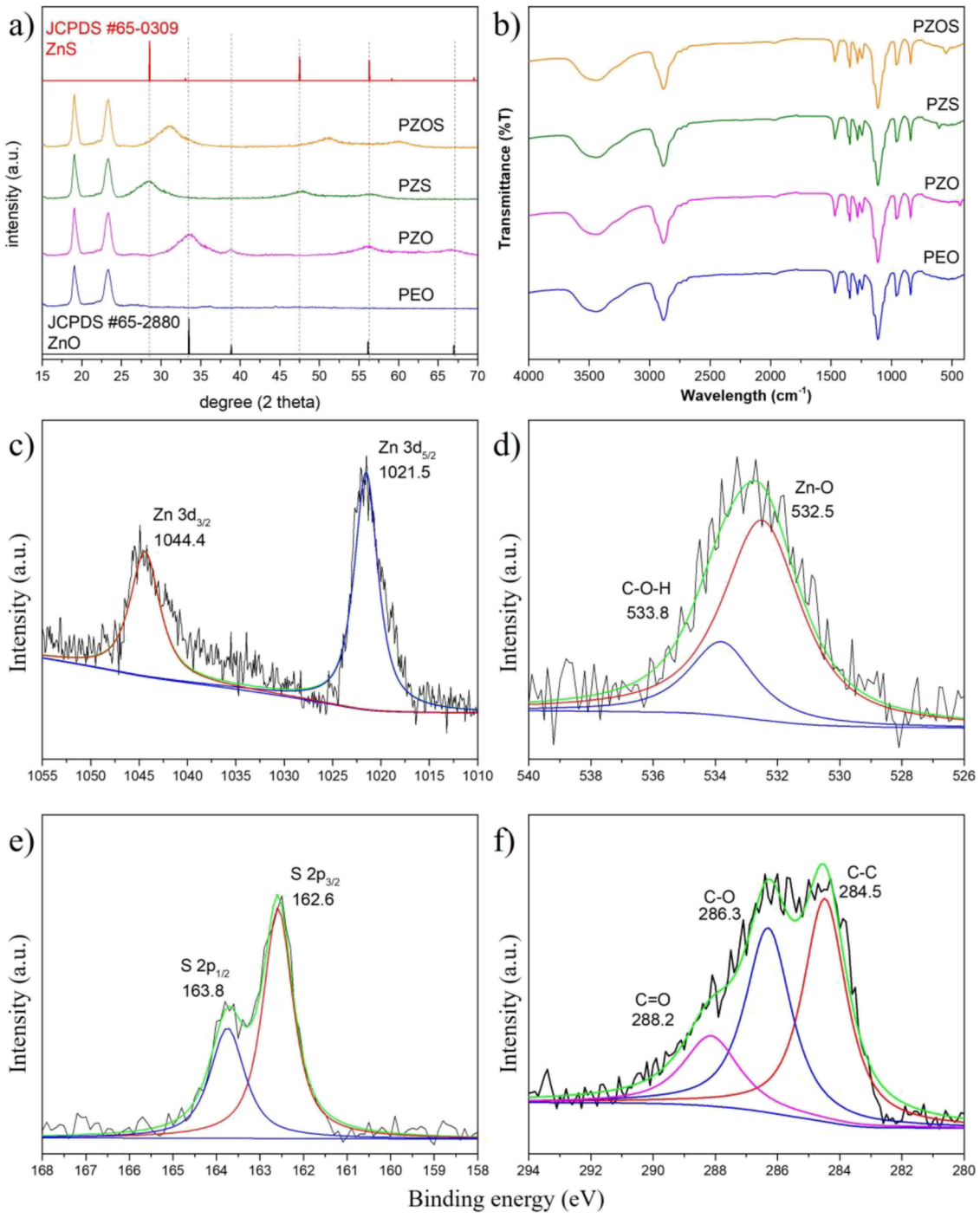


**Figure 2.** (a) Diffractogram of PEO, PZO, PZS, and PZOS nanofibers recorded from 15° to 70°. (b) FTIR spectra of PEO, PZO, PZS, and PZOS nanofibers were analyzed using the KBr method. The high-resolution XPS spectra of (c) Zn 3d, (d) O 1s, (e) S 2p, and (f) C 1s.

through electrochemical impedance spectroscopy (EIS) and transient photocurrent (TPC) analyses in a KCl 0.1 M solution.

**2.4. Photocatalytic Reduction of Nitrobenzene.** 50 mg of nanofiber was added in a photocatalytic reactor followed by adding 10 ppm of nitrobenzene (with volume of 400 mL $H_2O$ and 50 mL methanol). Prior to starting the photoreaction, the solution was purged using Ar gas for 30 min to eliminate the atmospheric gas, and a nanofiber sample was allowed in the solution under dark conditions to reach absorption−desorption equilibrium. Afterward, solar light was irradiated toward the photocatalytic reactor and an aliquot was taken every 15 min for UV−vis spectrum measurements. Moreover, the reusability of nanofibers was also investigated by testing the samples for five consecutive cycles for photocatalytic reduction of nitrobenzene.

## 3. RESULTS AND DISCUSSION

**3.1. Morphology of Nanofibers.** Figure 1a−c depicts the morphological images of pristine PZO, PZS, and PZOS nanofibers before the annealing process. As can be seen, there is no significant alteration for pristine PZO, PZS, and PZOS nanofibers where the samples exhibited smooth surfaces of



https://doi.org/10.1021/acsomega.3c05171
ACS Omega 2023, 8, 35328−35335

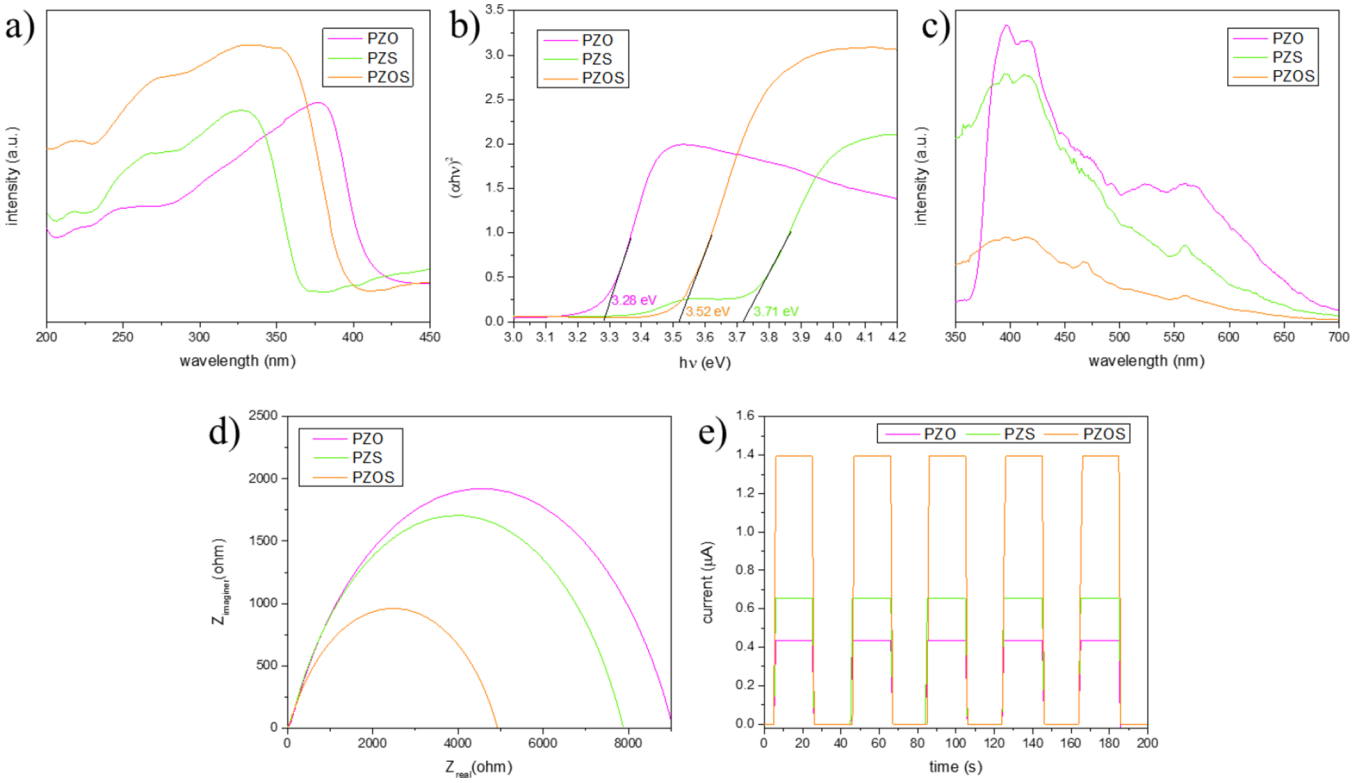


**Figure 3.** (a) DRS spectra, (b) Tauc plot, (c) PL, (d) EIS, and (e) TPC profiles of PZO, PZS, and PZOS nanofiber samples.

nanofibers. For annealed samples, a lot of tiny particles were observed on nanofiber surfaces revealing the existence of photocatalysts for ZnO, ZnS, and Zn(O,S) in Figure 1d–f, respectively. The average diameters of PZO, PZS, and PZOS nanofibers were found to be 20 ± 4.6 nm. Moreover, TEM analysis was conducted to further analyze the embedded Zn(O,S) in PEO nanofibers as shown in Figure 1g–i. Figure 1g indicates that the PZOS nanofiber is surrounded by tiny particles that are distributed uniformly and the average size of embedded Zn(O,S) photocatalyst is measured to be 5 ± 0.9 nm as shown in Figure 1h. Figure 1h also proved the agglomeration of particles showing the cohesion between PEO and Zn(O,S).[21] To confirm the successful synthesis of Zn(O,S) embedded in the PEO nanofiber, the lattice fringe analysis of a high-resolution TEM (HRTEM) image was performed. It is noticed that there are three different d-spacings found in the HRTEM image of PZOS (Figure 1i). The measured d-spacing values are 2.75, 2.87, and 3.09 Å located between those of ZnO and ZnS (111) planes confirming the phase of Zn(O,S).

**3.2. Crystallinity and Chemical Functionalities of Nanofibers.** The crystallinity of nanofiber samples was determined using XRD analysis and the diffractogram is shown in Figure 2a. Initially, there are two main peaks for PEO located at 19.1° and 23.3°. The PZO nanofiber exhibits peaks at 33.4°, 38.9°, 56.3°, and 66.9° corresponding to the crystal planes of (111), (200), (220), and (331), respectively, and these peaks are matched with the standard cubic ZnO (JCPDS card no. 65-2880). For the sulfurized sample (PZS), the arose peaks at 28.5° (111), 47.7° (220), and 56.2° (311) referred to zinc blende ZnS (JCPDS card no. 65-0309). Moreover, the successful embedment of Zn(O,S) in the PEO nanofiber was revealed by its diffractogram in Figure 2a in which the broad peak in PZOS shifted from 28.5° to higher 2$\theta$ of 31.1° and located between the peaks of cubic ZnO and zinc blende ZnS.

FTIR analysis was performed to determine the chemical functionalities contained in the composite nanofibers, and the FTIR spectra of PEO, PZO, PZS, and PZOS nanofibers are shown in Figure 2b. In the FTIR spectrum of PEO, the peaks at 3441 and 2883 $cm^{-1}$ referred to the functional groups of stretching -OH and CH $sp^3$, respectively.[22] The organic functionality peaks of bending $CH_2$, stretching C–O–C, bending C–H, and stretching C–C were located at 1445, 1106, 958, and 849 $cm^{-1}$, respectively.[20,23] In the presence of ZnO in PEO nanofibers, there was an additional peak observed at a wavelength of 438 $cm^{-1}$ corresponding to the stretching vibration of Zn–O.[24,25] Meanwhile, the presence of ZnS in PEO nanofibers was indicated by the Zn-S stretching vibration peak at 610 $cm^{-1}$.[26] Furthermore, the stretching vibration peak of Zn(O,S) was found at 554 $cm^{-1}$ in between those of ZnO and ZnS peaks.

The chemical states contained in the PZOS nanofiber were further determined using XPS analysis. Figure 2c,d shows the high-resolution XPS spectra of Zn, O, S, and C, respectively. There are two typical peaks of Zn which correspond to Zn $3d_{5/2}$ and $3d_{3/2}$ orbitals located at 1021.5 and 1044.4 eV, respectively.[27] The binding energy in O 1s orbital related to O lattice in Zn–O and C–O–H in the PEO polymer was located at 532.5 and 533.8 eV, respectively, as shown in Figure 2d.[27,28] The respective peak positions of S $2p_{3/2}$ and $2p_{1/2}$ were located at 162.6 and 163.8 eV as shown in Figure 2e.[29] In the C 1s XPS spectrum, it was found that there are three peaks referred to as C–C (284.5 eV), C–O (286.3 eV), and C═O (288.2 eV) as shown in Figure 2f.[27]

**3.3. Optical and Electrochemical Properties of Nanofibers.** The optical and electrochemical properties of the nanofiber samples were characterized using DRS, PL, EIS, and


https://doi.org/10.1021/acsomega.3c05171
ACS Omega 2023, 8, 35328–35335

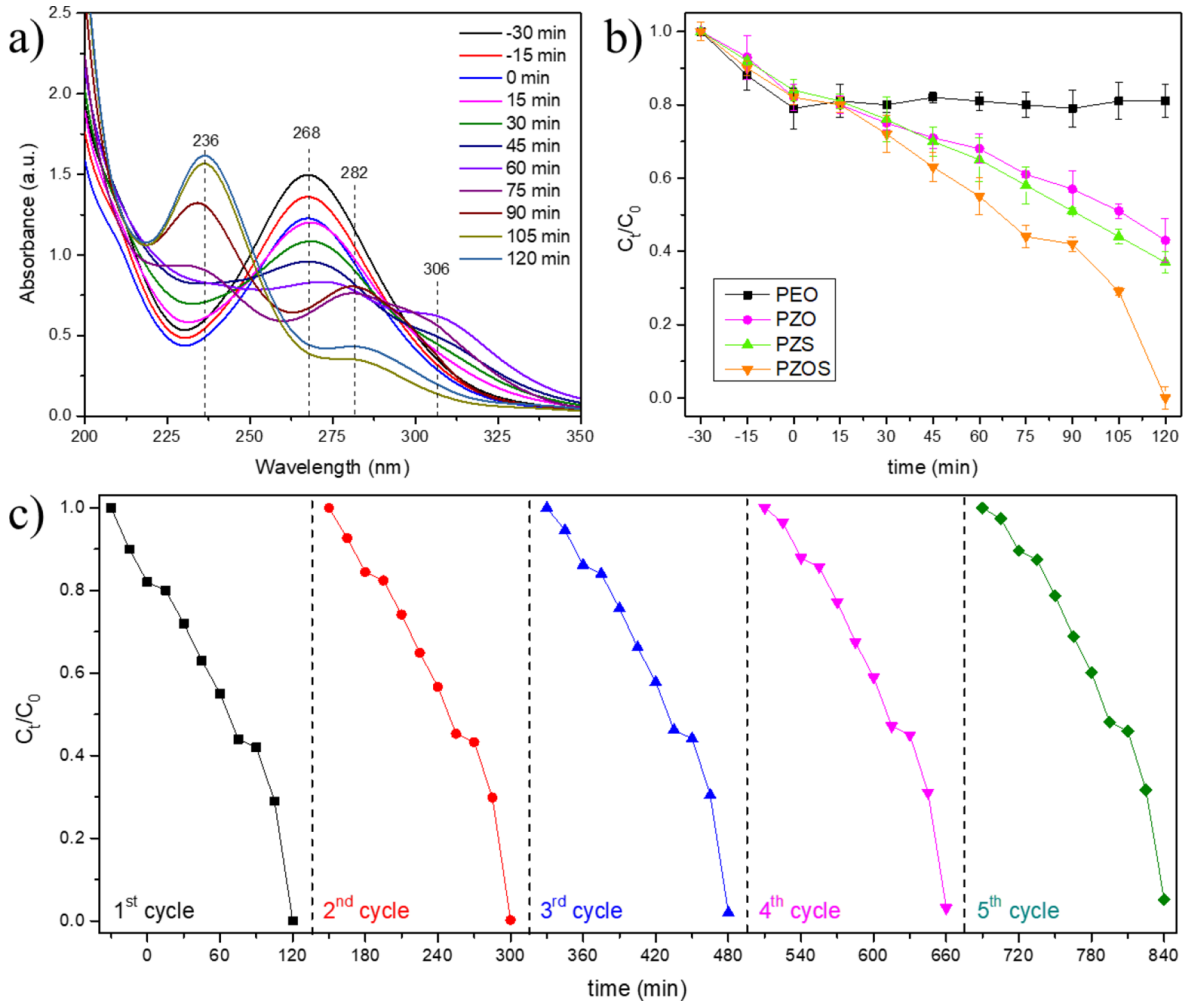


**Figure 4.** (a) UV−vis spectra of photocatalytic reduction of nitrobenzene to aniline by PZOS nanofiber under mild conditions. (b) Plots of $C_t/C_0$ vs reaction time of nitrobenzene degradation by PZO, PZS, and PZOS nanofibers. (c) Reusability performances of PZOS nanofiber for photocatalytic nitrobenzene reduction for five consecutive cycles.

TPC analyses. DRS analysis is an analytical technique that is used to study the optical absorption of samples and its converted Tauc plot is to determine the optical bandgap (Tauc bandgap). The DRS results showed that PZO, PZS, and PZOS nanofibers absorb light at 378, 328, and 348 nm, respectively (Figure 3a). Accordingly, the Tauc bandgap values of PZO, PZS, and PZOS nanofibers were found to be 3.28, 3.71, and 3.52 eV, respectively (Figure 3b). PL analysis was conducted to determine the recombination rate between photogenerated electrons and holes in the photocatalysts. As can be seen in Figure 3c, PZO and PZS possessed relatively high PL intensity denoting a shorter lifetime of photogenerated electrons and holes in ZnO and ZnS. After transitioning to Zn(O,S), the PL intensity of PZOS nanofiber drastically decreased 2.5-fold as compared to those of PZO and PZS nanofibers. These results demonstrated that photogenerated electrons and holes in PZOS could proceed with more efficient reduction and oxidation reactions. Moreover, the charge transfer resistance at the interfaces between the samples and electrolyte was measured using EIS analysis under a Randles electrical circuit. The smallest semicircle resistance of PZOS as shown in Figure 3d obviously leads to better charge transfer of photogenerated electrons and holes in the electrolyte as compared to those of PZO and PZS nanofibers. As photocatalysts require light as a driving force to generate electrons and holes, TPC analysis was carried out under an on−off condition as shown in Figure 3e. The TPC result also shows a good agreement with EIS results in which the PZOS nanofiber generates the highest photocurrent of ∼1.4 mA during the TPC measurement (Figure 3e).

**3.4. Photoreduction of Nitrobenzene.** Based on the optical and electrochemical measurements, it can be seen that PZOS demonstrated the most optimum photocatalytic properties compared to those of PZO and PZS nanofibers. Therefore, the PZOS nanofiber was applied for photocatalytic reduction of nitrobenzene under mild conditions with methanol as the hole scavenger. Initially, the peak of nitrobenzene was observed at 268 nm (Figure 4a).[30] Prior to starting the photocatalytic reaction, the PZOS nanofiber was allowed to absorb nitrobenzene until reached a saturated equilibrium condition (30 min). After saturation, the solar light source was irradiated to the photocatalytic reactor and an aliquot was taken every 15 min for UV−vis measurement. For the first hour, the nitrobenzene peak decreased gradually and at 60 min of photoreaction, the peak at 268 nm shifted toward a higher wavelength and a new shoulder peak appeared at 306 nm referred to as the intermediate of phenylhydroxylamine.[31] In this regard, nitrosobenzene intermediate was not detected due to its rapid conversion to phenylhydroxylamine.[32] Afterward,



https://doi.org/10.1021/acsomega.3c05171
ACS Omega 2023, 8, 35328−35335

there were two new peaks arose at 236 and 282 nm corresponding to the aniline compound, and the photoreduction of nitrobenzene to aniline by the PZOS nanofiber was completed within 2 h (Figure 4a).[33] In this study, we also compare PZOS nanofiber photocatalytic activity with PEO, PZO, and PZS nanofibers. The results show that the PEO nanofiber is unable to proceed with the photocatalytic reaction, whereas PZO and PZS nanofibers perform worse photoreduction performances (Figure 4b). To further study the robustness, the reusability of PZOS nanofiber was investigated by conducting five consecutive runs of photocatalytic nitrobenzene reduction. The reusability activities of PZOS nanofiber remained higher than 95% after five consecutive tests showing that the PZOS nanofiber has good durability (Figure 4c).

It was found that there are relatively fewer studies regarding the catalytic hydrogenation of nitrobenzene to aniline. Table 1

**Table 1. Comparison of Recent Literature on Catalytic Hydrogenation toward Nitrobenzene**

| materials | driving force | catalyst mass | [nitrobenzene] | reaction time | ref |
|---|---|---|---|---|---|
| Cu@C | $NaBH_4$ | 10 mg | 0.2 mmol | 10 min | 34 |
| palladium/carbon | $H_2$ gas | 0.1 g | 0.08 mol | 100 min | 35 |
| Pd/$TiO_2$ | UV light | 25 mg | 100 $\mu$mol | 18 h | 36 |
| Ni−Mg-co-doped Zn(O,S) | solar light | 10 mg | 30 ppm | 2 h | 37 |
| PZOS nanofiber | solar light | 50 mg | 10 ppm | 120 min | [this work] |

shows several works of literature that reported the catalytic hydrogenation of azobenzene to aniline using different catalysts. The synthesized PZOS nanofiber exhibited comparable performance as compared to those of other catalysts for nitrobenzene hydrogenation (Table 1).

### 3.5. Mechanism of Photocatalytic Hydrogenation.

The schematic illustration of PZOS nanofiber including the bandgap arrangement as well as the mechanism reaction for photoreduction of nitrobenzene to aniline on PZOS nanofiber are shown in Figure 5a,b, respectively. Upon light irradiation, electron-hole pairs were generated and the electron absorbed the energy from photon and excited to the conduction band leaving a hole in the valence band (Figure 5a).[38,39] Afterward, $e^-$ in the conduction band was ready to proceed with the reduction reaction involving $H^+$ to hydrogenate nitrobenzene to aniline; on the other hand, the oxidation reaction was executed by $h^+$ in the valence band.[40,41] As reported elsewhere, the conversion of nitrobenzene to aniline mainly involves two steps. First, the hydrogenation of nitrobenzene to phenylhydroxylamine through the intermediate of nitrosobenzene involving four $e^-$ and $H^+$. Then, the final product of aniline was obtained by further reduction by two more $e^-$ and $H^+$ as shown in Figure 5b.[42,43]

## 4. CONCLUSIONS

In summary, we demonstrated a fabrication of electrospun nanofiber mats embedded with Zn(O,S) photocatalyst for photocatalytic reduction of nitrobenzene to aniline under mild conditions under solar light irradiation. The successful synthesis of Zn(O,S) embedded in the PEO nanofiber is proved by HR-TEM and XRD analyses in which their lattice

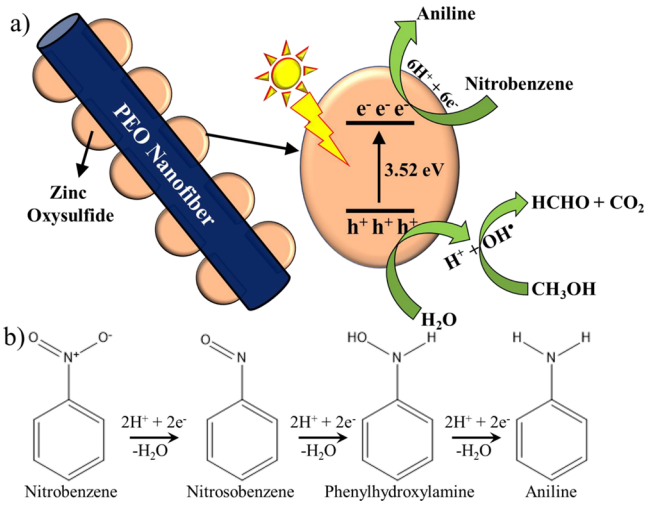


**Figure 5.** (a) Schematic illustration of PZOS nanofiber for photocatalytic reduction of nitrobenzene to aniline. (b) Reduction mechanism reaction of nitrobenzene to aniline.

fringes and diffraction planes are located in between those of ZnO and ZnS. This solid solution state of Zn(O,S) embedded in a nanofiber demonstrates a superior photocatalytic activity of nitrobenzene hydrogenation to aniline under solar light irradiation under mild conditions with methanol as a hole scavenger. The photocatalytic hydrogenation from nitrobenzene to aniline involves six $e^-$ and six $H^+$ converting nitrobenzene to nitrosobenzene, phenylhydroxylamine, and aniline. Finally, this work contributed not only to green recycling technology but also for industrial applications.

## AUTHOR INFORMATION


### Corresponding Authors

**Elvri Melliaty Sitinjak** − *Department of Chemical Engineering, Politeknik Teknologi Kimia Industri, Medan 20228, Indonesia;* orcid.org/0000-0002-7450-0329; Email: elvrimelliaty@ptki.ac.id

**Indra Masmur** − *Department of Chemistry, Faculty of Mathematics and Natural Sciences, Universitas Sumatera Utara, Medan 20155, Indonesia;* orcid.org/0000-0001-7853-4764; Email: intar76@yahoo.com, indramasmur@usu.ac.id

### Authors

**Poltak Evencus Hutajulu** − *Department of Palm Oil Agribusiness, Politeknik Teknologi Kimia Industri, Medan 20228, Indonesia*

**New Vita Mey Destty Marbun** − *Department of Palm Oil Agribusiness, Politeknik Teknologi Kimia Industri, Medan 20228, Indonesia*

**Golfrid Gultom** − *Department of Mechanical Engineering, Politeknik Teknologi Kimia Industri, Medan 20228, Indonesia*

Complete contact information is available at: https://pubs.acs.org/10.1021/acsomega.3c05171


### Notes

The authors declare no competing financial interest.



https://doi.org/10.1021/acsomega.3c05171
ACS Omega 2023, 8, 35328−35335

## ■ ACKNOWLEDGMENTS

The authors would like to thank Politeknik Teknologi Kimia Industri, Medan, and Universitas Sumatera Utara for the facilities and instrumentation to conduct the research.

## ■ REFERENCES

(1) Doluda, V. Y.; Filatova, A. E.; Sul'man, E. M.; Matveeva, V. G.; Mikhailov, S. P.; Sidorov, A. I.; Kosivtsov, Y. Y. Studying the Three-Phase Hydrogenation of Nitrobenzene to Aniline in the Presense of a Ruthenium Catalyst. *Catal. Ind.* **2018**, *10*, 328−334.
(2) Béchamp, A. J. 1854. Action des Protosels de Fer sur la Nitronaphthaline et la Nitrobenzine. *Ann. Chim. Phys.* [3], 42, 186-196.
(3) Driessen, R. T.; Kamphuis, P.; Mathijssen, L.; Zhang, R.; van der Ham, L. G. J.; van den Berg, H.; Zeeuw, A. J. Industrial Process Design for the Production of Aniline by Direct Amination. *Chem. Eng. Technol.* **2017**, *40*, 838−846.
(4) Wang, J.; Yuan, Z.; Nie, R.; Hou, Z.; Zheng, X. Hydrogenation of Nitrobenzene to Aniline over Silica Gel Supported Nickel Catalysts. *Ind. Eng. Chem. Res.* **2010**, *49*, 4664−4669.
(5) Torres, C.; Campos, C.; Fierro, J. L. G.; Oportus, M.; Reyes, P. Nitrobenzene Hydrogenation on Au/TiO2 and Au/SiO2 Catalyst: Synthesis, Characterization and Catalytic Activity. *Catal. Lett.* **2013**, *143*, 763−771.
(6) Moghaddam, M. M.; Pieber, B.; Glasnov, T.; Kappe, C. O. Immobilized Iron Oxide Nanoparticles as Stable and Reusable Catalysts for Hydrazine-Mediated Nitro Reductions in Continuous Flow. *ChemSusChem* **2014**, *7*, 3122−3131.
(7) Elessawy, N.; Elkady, M.; Elnouby, M.; Hamad, H. Microwave-assisted synthesis of new Cs doped ZrV2O7 nanorods with remarkably improved visible-light-driven photocatalytic performance. *Mater. Chem. Phys.* **2020**, *254*, No. 123494.
(8) Lee, G.-J.; Wu, J. J. Recent developments in ZnS photocatalysts from synthesis to photocatalytic applications — A review. *Powder Technol.* **2017**, *318*, 8−22.
(9) Paraguay-Delgado, F.; Hermida-Montero, L. A.; Morales-Mendoza, J. E.; Durán-Barradas, Z.; Mtz-Enriquez, A. I.; Pariona, N. Photocatalytic properties of Cu-containing ZnO nanoparticles and their antifungal activity against agriculture-pathogenic fungus. *RSC Adv.* **2022**, *12*, 9898−9908.
(10) De, A. K.; Kumar, U.; Jatav, N.; Sinha, I. Cd-doped Ag2O/BiVO4 visible light Z-scheme photocatalyst for efficient ciprofloxacin degradation. *RSC Adv.* **2022**, *12*, 35639−35648.
(11) Zhang, Y.; Xu, X. LaTaON2−BaTaO2N solid solutions for photocatalytic water oxidation. *Inorg. Chem. Front.* **2021**, *8*, 3723−3732.
(12) Tang, J.; Xue, Y.; Ma, C.; Zhang, S.; Li, Q. Facile preparation of BiOI/T-ZnOw p−n heterojunction photocatalysts with enhanced removal efficiency for rhodamine B and oxytetracycline. *New J. Chem.* **2022**, *46*, 13010−13020.
(13) Nie, J.; Schneider, J.; Sieland, F.; Zhou, L.; Xia, S.; Bahnemann, D. W. New insights into the surface plasmon resonance (SPR) driven photocatalytic H2 production of Au−TiO2. *RSC Adv.* **2018**, *8*, 25881−25887.
(14) Liu, H.; Yuan, J.; Jiang, Z.; Shangguan, W.; Einaga, H.; Teraoka, Y. Novel photocatalyst of V-based solid solutions for overall water splitting. *J. Mater. Chem.* **2011**, *21*, 16535−16543.
(15) Chai, Y.; Li, L.; Lu, J.; Li, D.; Shen, J.; Zhang, Y.; Liang, J.; Wang, X. Germanium-substituted Zn2TiO4 solid solution photocatalyst for conversion of CO2 into fuels. *J. Catal.* **2019**, *371*, 144−152.
(16) Chen, Y.-Y.; Kuo, C.-C.; Chen, B.-Y.; Chiu, P.-C.; Tsai, P.-C. Multifunctional polyacrylonitrile-ZnO/Ag electrospun nanofiber membranes with various ZnO morphologies for photocatalytic, UV-shielding, and antibacterial applications. *J. Polym. Sci., Part B: Polym. Phys.* **2015**, *53*, 262−269.
(17) Lin, C. C.; Jiang, D.-H.; Kuo, C.-C.; Cho, C.-J.; Tsai, Y.-H.; Satoh, T.; Su, C. Water-Resistant Efficient Stretchable Perovskite-Embedded Fiber Membranes for Light-Emitting Diodes. *ACS Appl. Mater. Interfaces* **2018**, *10*, 2210−2215.
(18) Liang, F.-C.; Kuo, C.-C.; Chen, B.-Y.; Cho, C.-J.; Hung, C.-C.; Chen, W.-C.; Borsali, R. RGB-Switchable Porous Electrospun Nanofiber Chemoprobe-Filter Prepared from Multifunctional Copolymers for Versatile Sensing of pH and Heavy Metals. *ACS Appl. Mater. Interfaces* **2017**, *9*, 16381−16396.
(19) Venkatesan, M.; Veeramuthu, L.; Liang, F.-C.; Chen, W.-C.; Cho, C.-J.; Chen, C.-W.; Chen, J.-Y.; Yan, Y.; Chang, S.-H.; Kuo, C.-C. Evolution of electrospun nanofibers fluorescent and colorimetric sensors for environmental toxicants, pH, temperature, and cancer cells − A review with insights on applications. *Chem. Eng. J.* **2020**, *397*, No. 125431.
(20) Masmur, I.; Perangin-angin, S.; Sembiring, H.; Tarigan, A. H.; Ginting, J.; Barus, D. A.; Ginting, M. Effect of Different Composition of Polyethylene Oxide-Polypyrrole (PEO-PPy) Nanofiber Mats on Antibacterial and Biocompatibility Properties. *ChemistrySelect* **2022**, *7*, No. e202201346.
(21) Samy, M.; Ibrahim, M. G.; Gar Alalm, M.; Fujii, M.; Diab, K. E.; ElKady, M. Innovative photocatalytic reactor for the degradation of chlorpyrifos using a coated composite of ZrV2O7 and graphene nano-platelets. *Chem. Eng. J.* **2020**, *395*, No. 124974.
(22) Venkatesan, M.; Chandrasekar, J.; Liang, F.-C.; Lin, W.-C.; Chen, W.-C.; Cho, C.-J.; Chen, Y.-T.; Lee, W.-Y.; Su, C.; Zhou, Y.; Lai, Y.-C.; Kuo, C.-C. Surface-enhanced fully nanofiber-based self-cleanable ultraviolet resistive triboelectric energy harvester for wearable smart garments. *Nano Energy* **2023**, *113*, No. 108556.
(23) Farea, M. O.; Abdelghany, A. M.; Oraby, A. H. Optical and dielectric characteristics of polyethylene oxide/sodium alginate-modified gold nanocomposites. *RSC Adv.* **2020**, *10*, 37621−37630.
(24) da Silva-Neto, M. L.; de Oliveira, M. C. A.; Dominguez, C. T.; Lins, R. E. M.; Rakov, N.; de Araújo, C. B.; Menezes, L. D. S.; de Oliveira, H. P.; Gomes, A. S. L. UV random laser emission from flexible ZnO-Ag-enriched electrospun cellulose acetate fiber matrix. *Sci. Rep.* **2019**, *9*, 11765.
(25) Elkady, M. F.; Hassan, H. S. Photocatalytic Degradation of Malachite Green Dye from Aqueous Solution Using Environmentally Compatible Ag/ZnO Polymeric Nanofibers. *Polymers* **2021**, *13*, 2033.
(26) Khodamorady, M.; Bahrami, K. Fe3O4@BNPs@ZnO−ZnS as a novel, reusable and efficient photocatalyst for dye removal from synthetic and textile wastewaters. *Heliyon* **2023**, *9*, No. e16397.
(27) Qu, G.; Fan, G.; Zhou, M.; Rong, X.; Li, T.; Zhang, R.; Sun, J.; Chen, D. Graphene-Modified ZnO Nanostructures for Low-Temperature NO2 Sensing. *ACS Omega* **2019**, *4*, 4221−4232.
(28) Wu, Y.; Lin, Y.; Xu, J. Synthesis of Ag−Ho, Ag−Sm, Ag−Zn, Ag−Cu, Ag−Cs, Ag−Zr, Ag−Er, Ag−Y and Ag−Co metal organic nanoparticles for UV-Vis-NIR wide-range bio-tissue imaging. *Photochem. Photobiol. Sci.* **2019**, *18*, 1081−1091.
(29) Tai, G.; Zeng, T.; Yu, J.; Zhou, J.; You, Y.; Wang, X.; Wu, H.; Sun, X.; Hu, T.; Guo, W. Fast and large-area growth of uniform MoS2 monolayers on molybdenum foils. *Nanoscale* **2016**, *8*, 2234−2241.
(30) Jeong, S.; Lee, H.; Park, H.; Jeon, K.-J.; Park, Y.-K.; Jung, S.-C. Rapid photocatalytic degradation of nitrobenzene under the simultaneous illumination of UV and microwave radiation fields with a TiO2 ball catalyst. *Catal. Today* **2018**, *307*, 65−72.
(31) Wang, J.; Ge, Z.; Pei, L.; Kong, P.; Wang, R.; Zhu, P.; Liu, M.; Gu, X.; Zheng, Z. ZnNb2O6 fibre surface as an efficiently product-selective controller for the near-UV-light-induced nitrobenzene reduction reaction. *Catal. Sci. Technol.* **2019**, *9*, 6681−6690.
(32) Favre, T. L. F.; Seijsener, P. J.; Kooyman, P. J.; Maltha, A.; Zuur, A. P.; Ponec, V. Selective reduction of nitrobenzene to nitrosobenzene on oxidic catalysts. *Catal. Lett.* **1988**, *1*, 457−460.
(33) Wu, W.; Lin, R.; Shen, L.; Liang, R.; Yuan, R.; Wu, L. Highly efficient visible-light-induced photocatalytic hydrogenation of nitrobenzene to aniline in water. *RSC Adv.* **2013**, *3*, 10894−10899.
(34) Tang, J.; Zhang, S.; Chen, X.; Zhang, L.; Du, L.; Zhao, Q. Highly Efficient Catalytic Reduction of Nitrobenzene Using Cu@C Based on a Novel Cu–MOF Precursor. *Catalysts* **2023**, *13*, 956.


https://doi.org/10.1021/acsomega.3c05171
*ACS Omega* 2023, 8, 35328−35335

(35) Gelder, E. A.; Jackson, S. D.; Lok, C. M. The hydrogenation of nitrobenzene to aniline: a new mechanism. *Chem. Commun.* **2005**, 522−524.
(36) Zhou, B.; Song, J.; Zhou, H.; Wu, L.; Wu, T.; Liu, Z.; Han, B. Light-driven integration of the reduction of nitrobenzene to aniline and the transformation of glycerol into valuable chemicals in water. *RSC Adv.* **2015**, *5*, 36347−36352.
(37) Abdullah, H.; Shuwanto, H.; Kuo, D.-H. Multifunctional Ni−Mg bimetal-activated Zn(O,S) for hydrogen generation and environmental remediation with simulated solar-light irradiation. *Catal. Sci. Technol.* **2021**, *11*, 7200−7216.
(38) Rani, B.; Nayak, A. K.; Sahu, N. K. Fundamentals principle of photocatalysis. In *Nanostructured Materials for Visible Light Photocatalysis*, Nayak, A. K.; Sahu, N. K., Eds.; Elsevier, 2022; pp 1−22.
(39) Yang, X.; Wang, D. Photocatalysis: From Fundamental Principles to Materials and Applications. *ACS Appl. Energy Mater.* **2018**, *1*, 6657−6693.
(40) Ma, D.; Zhai, S.; Wang, Y.; Liu, A.; Chen, C. TiO2 Photocatalysis for Transfer Hydrogenation. *Molecules* **2019**, *24*, 330.
(41) Tamaki, Y.; Furube, A.; Murai, M.; Hara, K.; Katoh, R.; Tachiya, M. Direct Observation of Reactive Trapped Holes in TiO2 Undergoing Photocatalytic Oxidation of Adsorbed Alcohols: Evaluation of the Reaction Rates and Yields. *J. Am. Chem. Soc.* **2006**, *128*, 416−417.
(42) Daems, N.; Wouters, J.; Van Goethem, C.; Baert, K.; Poleunis, C.; Delcorte, A.; Hubin, A.; Vankelecom, I. F. J.; Pescarmona, P. P. Selective reduction of nitrobenzene to aniline over electrocatalysts based on nitrogen-doped carbons containing non-noble metals. *Appl. Catal., B* **2018**, *226*, 509−522.
(43) Mahata, A.; Rai, R. K.; Choudhuri, I.; Singh, S. K.; Pathak, B. Direct vs. indirect pathway for nitrobenzene reduction reaction on a Ni catalyst surface: a density functional study. *Phys. Chem. Chem. Phys.* **2014**, *16*, 26365−26374.



https://doi.org/10.1021/acsomega.3c05171
*ACS Omega* 2023, 8, 35328−35335